IL NUOVO CIMENTO **43 C** (2020) 116
DOI 10.1393/ncc/i2020-20116-2

COMMUNICATIONS: SIF Congress 2019

Pressure evolution of the optical phonons of $MoTe_2$

E. STELLINO

Università degli studi di Perugia - Perugia, Italy

received 28 January 2020

Summary. — In this work, we report a study on the evolution of the $MoTe_2$ phonons under pressure, performed through optical spectroscopy on bulk samples. Raman and infrared measurements were carried out at room temperature (RT) up to ∼20 GPa. The analysis of the phonon frequencies as a function of pressure confirms the absence of structural transition, already observed in the literature. The abrupt broadening of the Raman peaks above 18 GPa suggests an increase of the charge carriers, also supported by the rapid decrease of the infrared peak area in the range 13–19 GPa. The asymmetric line-shape of the infrared peak at low pressure has been interpreted in the framework of the Fano theory, in analogy to the results obtained for graphene, and related to the presence of doping levels in the band structure.

1. – Introduction

Transition-Metal Dichalcogenides (TMDs) are layered crystals with stoichiometry MX_2, where M is a transition metal atom and X is a chalcogen element [1, 2]. Since the intra-layer covalent bonds are far stronger than the inter-layer van der Waals forces, few-layer down to mono-layer samples can be exfoliated from the crystal bulk, obtaining systems with almost two-dimensional features [3, 4].

In Mo-based TMDs semiconductors, the interplay between adjacent layers is a key feature in determining the electronic properties of the sample. Scaling down the number of layers weakens their mutual interaction inducing an expansion of the inter-layer distance and a significant variation in the crystal band-structure. Indeed, a progressive enlargement of the band-gap is observed as the number of layers reduces, and an indirect-to-direct band-gap crossover arises when going from bi-layer to mono-layer samples (where the inter-layer distance actually goes to infinity) [5-7]. Conversely, the application of pressure, which compresses the lattice structure and in particular the distance between the planes, allows investigating the response of bulk crystals when the inter-layer interaction increases, analysing the sample under conditions inaccessible by thickness-dependent studies. In particular, pressure increases the overlap between the

electronic wavefunctions driving non-trivial changes in the electronic band-structure such as semiconductor-to-metal transitions.

Among Mo-based semiconductors, $MoTe_2$ exhibits an indirect band-gap of $\sim$1 eV and a direct gap of $\sim$1.1 eV in the mono-layer case [8]. Compared to the most widely studied MoS_2 and $MoSe_2$, whose band-gaps lie in the visible region [8], the $MoTe_2$ gap energy is smaller and makes this crystal suitable for optoelectronic devices also in the near-infrared range [9-11].

DFT calculations have found that the $MoTe_2$ lattice structure does not appreciably change up to 50 GPa [12], in agreement with high-pressure Raman results [13-15], carried out to $\sim$30 GPa. As for the electronic structure, Riflíková *et al.* predicted a semiconductor-to-semimetal transition in the range 13–19 GPa [16]. Transport measurements have then provided evidence of the transition to the metallic state between $\sim$10 and 13 GPa [13, 15]. In this framework, we report a high-pressure study on bulk samples of $MoTe_2$ performed through Raman and Far-Infrared (FIR) spectroscopy. Our approach allows inferring the pressure dependence of electronic and structural properties by taking into account the evolution of optical phonons under pressure.

2. – Raman measurements

A $MoTe_2$ crystal, provided by HQ graphene, was exfoliated to obtain a fresh-cut sample. RT Raman measurements were carried out by means of the Horiba LabRAM HR Evolution micro spectrometer, and a DIACELL diamond-anvil cell was employed to cover the 0–23 GPa pressure range. The gasket was made of a 250 μm thick steel foil, with a sample chamber of 100 μm diameter and 50 μm height. A small $MoTe_2$ flake was loaded inside the gasket hole together with NaCl powder, used as hydrostatic medium. The lateral dimensions of the crystal were $\sim 40 \times 40\,\mu m^2$; its thickness $d \sim 10\,\mu$m allowed us to safely work in the bulk limit since the inter-layer distance in $MoTe_2$ is $\sim$0.7 nm. A ruby sphere was also put into the sample chamber to measure the pressure through the standard ruby fluorescence techniques. By using the confocal microscope with the 50$\times$ long working distance objective, we obtained a laser spot about 2 μm wide at the sample surface.

A polynomial background has been subtracted to highlight the phonon-Raman response measured as a function of the pressure. The phonon contribution is shown in fig. 1(a) at selected pressures. Notice that the spectra collected over the low-pressure range (0–2 GPa) are not reported owing to the low signal-to-noise ratio, since, on squeezing the diamonds, $MoTe_2$ layers have an easier alignment between the pressure synthesized NaCl pellet and the inner face of the diamond culet.

In ref. [17] we carefully measured the ambient pressure Raman spectra of a sample of $MoTe_2$ belonging to the same batch as the present one. In that case, particular attention was devoted to the polarization dependence of the Raman response [17]. According to the literature, in ref. [17] and in the present paper at low pressure, three main peaks have been observed at $\sim 25\,cm^{-1}$, $\sim 190\,cm^{-1}$ and $\sim 230\,cm^{-1}$ and ascribed to the E^2_{2g} (in-plane), A_{1g} (out-of-plane) and E^1_{2g} (in-plane) vibrational modes, respectively.

The three peaks have been fitted with a Voigt profile to account for *disorder* effects (pressure gradients and local misalignment) and the *natural* peak profile. The best-fit parameters obtained for the central frequencies and the full width at half-maximum (FWHM) have been plotted as a function of the pressure, together with the ratio between the intensities of the out-of-plane mode and the high-frequency in-plane mode $I(A_{1g})/I(E^1_{2g})$; see figs. 1(b), (c), (d), (e).

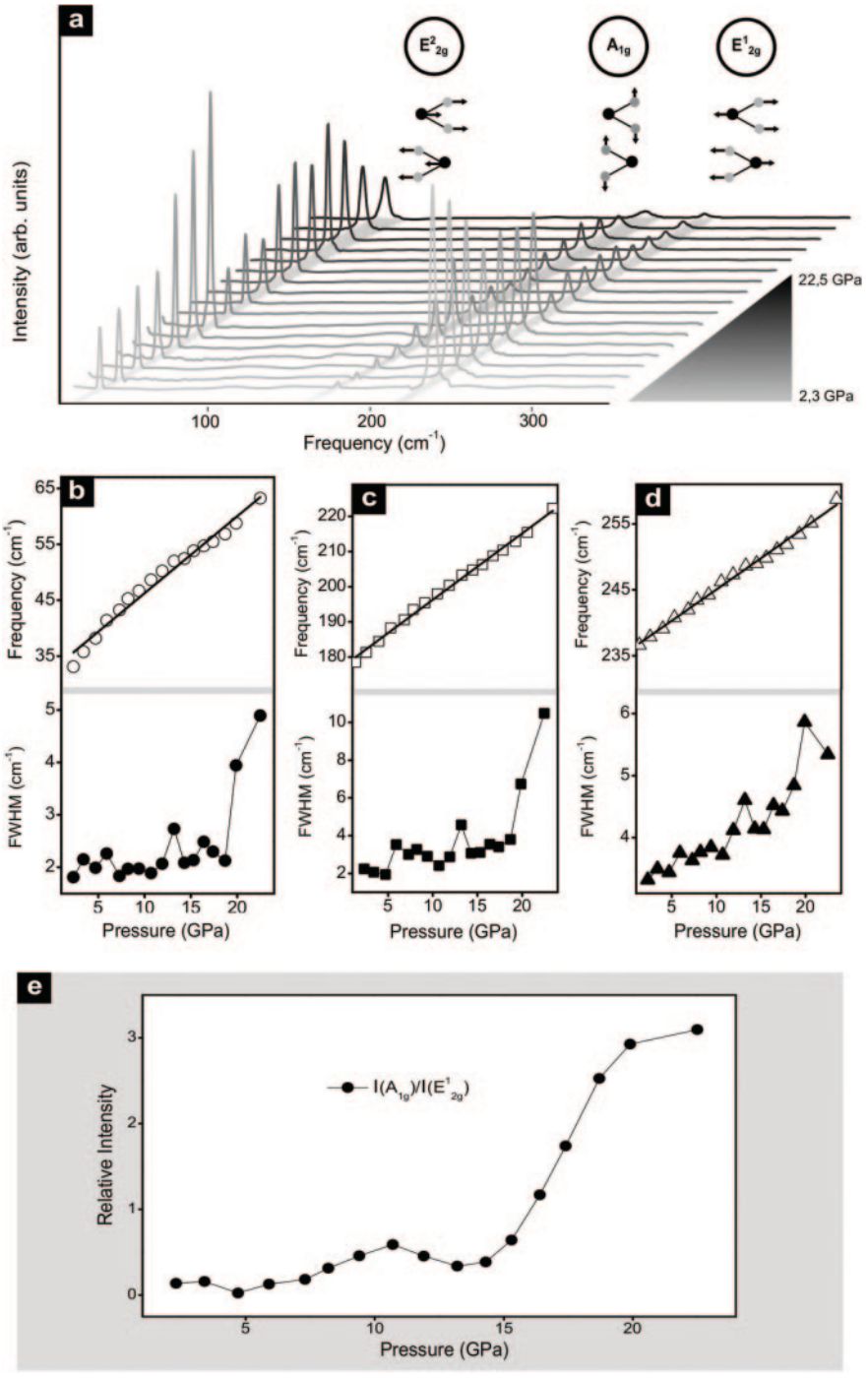

Fig. 1. – Panel (a): $MoTe_2$ Raman spectra in the range 2–23 GPa. Panels (b), (c), (d): evolution of the peak position and FWHM as a function of the pressure for the E^2_{2g} (b), A_{1g} (c), E^1_{2g} (d) modes. Panel (e): evolution of the relative intensity $I(A_{1g})/I(E^1_{2g})$ as a function of the pressure.

It is worth noticing that, as mentioned in ref. [17], the absolute intensities of the three main peaks show a strong dependence on polarization, that is from the angles between the laser beam polarization (linear polarization) and the three crystal axes. At each working pressure, the $MoTe_2$ crystal can change its alignment with respect to the fixed polarization direction, the laser beam cannot be directed exactly on the same portion of the sample surface and a slightly different focus can occur. All these effects can produce actually uncontrolled variation of absolute intensities of the three analyzed Raman peaks. For this reason, we restricted the analysis to the peak frequencies, FWHM and relative intensities only.

As the pressure is increased, the central frequency of all the peaks continuously shifts toward higher values, as expected for volume compression. Nevertheless, the peak pattern remains basically unchanged in agreement with the absence of structural transitions already observed and predicted in the literature [12-15], see fig. 1(a). The pressure dependence of the peak position has been linearly fitted to extrapolate the peak frequency at ambient conditions ($\hat{\nu}_0$) and its rate of increase as a function of pressure ($\partial\hat{\nu}/\partial P$). The fitting parameters are reported in table I. Differences in the $\partial\hat{\nu}/\partial P$ values can be ascribed to the different vibrational directions of the modes: since in TMDs the vdW inter-layer interaction is far weaker than the covalent intra-layer bonds, out-of-plane phonons, as A_{1g}, are more sensitive to the lattice compression than in-plane modes, like E^1_{2g} and E^2_{2g}. Notice that, at variance with the high-frequency phonons, E^2_{2g} pressure pattern visibly departs from the linear fit. For this reason, we also performed a *sublinear* fit [18], with the function $\hat{\nu}(P) = C[\frac{A}{B} \cdot P + 1]^B$, obtaining $A = 0.14\,\mathrm{GPa}^{-1}$, $B = 0.38$, $C = 26.4\,\mathrm{cm}^{-1}$.

While the analysis of the peak frequencies gives us information on the effect of pressure on the inter-, intra-layer vibrational modes, the peak FWHM is associated to interactions and charge transfer processes, whose onset reduces the phonon lifetime and therefore broaden the phonon peak profile. In the present case, as shown in figs. 1(b), (c), (d), all the three peaks undergo an abrupt widening above 19 GPa indicating an increase of the carrier density possibly associated with a metallization process. Moreover, the ratio between A_{1g} and E^1_{2g} intensities, $I(A_{1g})/I(E^1_{2g})$, reported in fig. 1(e), increases above 13 GPa suggesting a pressure-induced transfer of charge carriers in the out-of-plane direction.

TABLE I. – *Intercepts, ν_0 (peak position at $P = 0$), and slopes, $\partial\hat{\nu}/\partial P$, obtained by a linear fit of the pressure dependence of the frequencies of the four optical phonon peaks. The errors on the intercept and the slopes were estimated exploiting the maximum and minimum slope method, assuming an uncertainty of $\pm 2\,cm^{-1}$ on the peak position and of 0.2 GPa on the pressure value.*

Phonon	$\hat{\nu}_0\,(\mathrm{cm}^{-1})$ Present work	$\hat{\nu}_0\,(\mathrm{cm}^{-1})$ ref. [14]	$\partial\hat{\nu}/\partial P\ (\mathrm{cm}\cdot\mathrm{GPa})^{-1}$ Present work	$\partial\hat{\nu}/\partial P\ (\mathrm{cm}\cdot\mathrm{GPa})^{-1}$ refs. [17, 21]
E^2_{2g}	33 ± 2	26.9	1.5 ± 0.3	–
A_{1g}	175 ± 2	173.3	2.2 ± 0.2	1.7
E^1_{2g}	235 ± 2	234	1.1 ± 0.2	1
E_{1u}	240 ± 2	234.5	1.1 ± 0.3	–

3. – Far-Infrared measurements

RT Far-Infrared (FIR) measurements were performed at the AILES beamline of synchrotron SOLEIL [19, 20] over the 0–20 GPa range. In the DAC, diamonds with culet of 500 μm were separated by a pre-indented stainless-steel 50 μm thick gasket, in which a hole with 250 μm diameter was drilled. The Bruker IFS 125 HR interferometer, coupled to the synchrotron source, was equipped with a multi-layer 6 μm beamsplitter and a liquid helium bolometer. Polyethene powder was used as pressure-transmitting medium, allowing reliable measurements over the 100–600 cm^{-1} spectral range. As for Raman measurements, the exfoliated sample was positioned in the hole together with the pressure transmitting medium and a ruby chip, to measure the pressure through the ruby fluorescence technique. The sample lateral dimensions were $\sim 50 \times 50$ μm, while its thickness was ~ 2 μm, allowing us to work in the bulk limit.

Background intensity $I_0(\hat{\nu})$ was collected with the DAC filled by only polyethene powder. From the intensity $I(\hat{\nu})$ transmitted when the $MoTe_2$ sample is loaded in the cell, the absorbance spectrum $A(\hat{\nu}) = -\ln[I(\hat{\nu})/I_0(\hat{\nu})]$ was obtained at different pressures, from 1 to 19 GPa. Intense oscillating fringes, due to multiple reflections between the diamond surfaces through the Polyethylene powder, were observed in both the $I_0(\hat{\nu})$ and the $I(\hat{\nu})$ spectra, see fig. 2. The reduced number of oscillation, the intrinsic spectral noise, the frequency dependence of both the period and the amplitude (mainly) of the oscillations prevent an effective subtraction in the absorbance spectra. However, besides the oscillation, a sharp peak is evident at $\sim 235\,cm^{-1}$ and has been assigned to the E_{1u} vibrational mode [21]. In fig. 3(a) we report the $A(\hat{\nu})$ spectra in an enlarged scale around the E_{1u} peak. The values of both the central frequencies and the peak areas are shown in fig. 3(b) as a function of the pressure. In analogy to what we have seen for the Raman peaks, the E_{1u} position regularly shifts toward higher frequencies on increasing pressure confirming the absence of structural transitions observed in the literature. In table I we have reported the parameters of the linear fit performed over the E_{1u} frequency

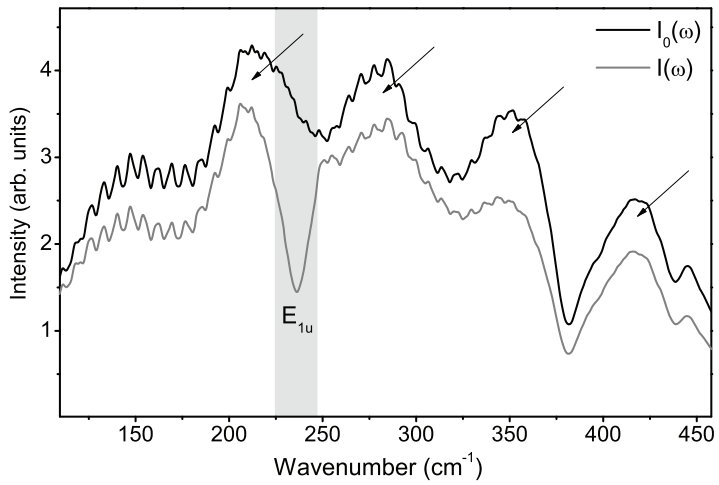

Fig. 2. – Background intensity ($I_0(\hat{\nu})$) and transmitted intensity ($I(\hat{\nu})$) at 1 GPa. Black arrows indicate the large interference fringes in the two spectra. Grey rectangle highlights the E_{1u} peak in the transmitted intensity.

trend shown in fig. 3(b). It can be noticed that, since E_{1u} represents the anti-symmetric counterpart of the Raman-active symmetric E^1_{2g} mode, these two phonons are almost degenerate in energy at ambient pressure and show the same pressure dependence; see table I.

At variance with the Raman measurements, where the peak absolute intensities were difficult to analyze, as discussed in the previous paragraph, the intensity of the infrared E_{1u} peak exhibits a clear and physically relevant trend under pressure. As shown in fig. 3(b), in fact, the peak area remains almost constant up to ∼13 GPa and then rapidly decreases, indicating an increase of the charge carriers that screens the phonon excitation. This result is in good agreement with the Raman peak broadening observed above 18 GPa and with the transport measurements found in the literature, which indicate the onset of a metallic behaviour at ∼12–13 GPa [13, 15].

Although the presence of interference fringes prevents an effective analysis of the E_{1u} peak profile, by comparing the E^1_{2g} and E_{1u} line-shapes at low pressure, it is quite evident that the latter shows a rather asymmetric peak with a pronounced dip on the

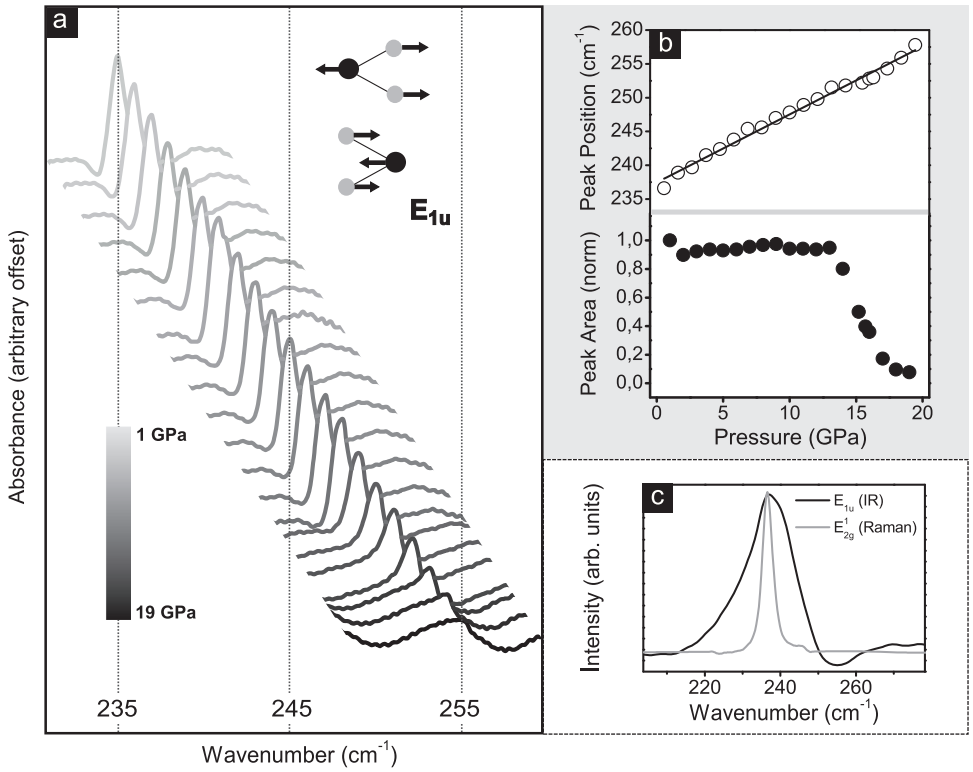

Fig. 3. – (a) Absorbance spectra in the frequency region around the E_{1u} peak; offsets have been arbitrary shifted to highlight the peak evolution under pressure. (b) On the top, peak position as a function of the pressure; the solid line represents the linear fit of the experimental data. On the bottom, peak area as a function of the pressure normalized to the 1 GPa value. (c) Line-shapes of IR-active E_{1u}, in black, and Raman-active E^1_{2g}, in red, at 2 GPa; the intensities have been rescaled to ease the comparison between the two peak profiles.

high-frequency side of the spectrum, see fig. 3(c). In the literature [22], a very similar behaviour has been observed for graphene phonons and has been interpreted in the framework of the Fano theory [23]. The presence of n-type doping levels in the $MoTe_2$ electronic bands and the close resemblance between the lattice structure of graphene and TMDs make these results reasonably extensible to our sample, explaining the different peak-profiles observed in FIR and Raman spectra.

4. – Conclusion

In this work, we report an investigation of the $MoTe_2$ properties under pressure through optical spectroscopies. In Raman spectra, the regular trend of the peaks up to 23 GPa is coherent with the absence of structural transitions indicated in the literature, while the abrupt broadening of the peak FWHM above 18 GPa is possibly related to the onset of the metallization process. The $I(A_{1g})/I(E^1_{2g})$ ratio increase above 13 GPa has been interpreted as the consequence of a charge carriers transfer in the out-of-plane direction.

In FIR spectra, the E_{1u} position evolves under pressure in analogy to the E^1_{2g} peak, *i.e.*, its Raman-active symmetric counterpart. As for the E_{1u} area, it rapidly decreases above 13 GPa suggesting an increase of the carrier density, which may be responsible for the screening of the phonon excitation. This result is in agreement with previous transport measurements that provide evidence of an enhancement of the charge carrier density at 12–13 GPa [13, 15]. Moreover, further measurements in the near-infrared are in the process of being analysed and could give us the possibility to correlate the pressure evolution of the energy band-gap to the response of optical phonons.

A comparison between the optical in-plane modes, E^1_{2g} Raman-active and E_{1u} IR-active at low pressure revealed that the latter exhibits a rather asymmetric profile. On the basis of the results obtained for graphene phonons, this effect has been explained in the framework of the Fano theory and has been related to the presence of doping levels in the sample band-structure.

REFERENCES

[1] Kobolov A. V. and Tominaga J., *Two-Dimensional Transition-Metal Dichalcogenides* (Springer International Publishing) 2016.

[2] Manzeli S., Ovchinnikov D., Pasquier D., Yazyev O. and Kis A., *Nat. Rev. Mater.*, **2** (2017) 17033.

[3] Li X., Tao L., Chen Z., Fang H., Li X., Wang X., Xu J. B. and Zhu H., *Appl. Phys. Rev.*, **4** (2017) 021306.

[4] Yuan L., Ge J., Peng X., Zhang Q., Wu Z., Jian Y., Xiong X., Yin H. and Han J., *AIP Adv.*, **6** (2016) 125201.

[5] Yun W. S., Han S. W., Hong S. C., Kim I. G. and Lee J. D., *Phys. Rev. B*, **85** (2012) 033305.

[6] Zhang Y. *et al.*, *Nat. Nanotechnol.*, **9** (2013) 111.

[7] Mak K. F., Lee C., Hone J., Shan J. and Heinz T. F., *Phys. Rev. Lett.*, **105** (2010) 136805.

[8] Wang Q. H., Kalantar-Zadeh K., Kis A., Coleman J. N. and Strano M. S., *Nat. Nanotechnol.*, **7** (2012) 699.

[9] Pradhan N. R. *et al.*, *ACS Nano*, **8** (2014) 5911.

[10] Huang H. *et al.*, *Nanotechnology*, **27** (2016) 44520.

[11] Yu W., Li S., Zhang Y., Ma W., Tian S., Yuan J., Fu K. and Bao Q., *Small*, **13** (2017) 1700268.
[12] Kohulák O. and Martoňák R., *Phys. Rev. B*, **95** (2017) 054105.
[13] Zhao X. M., Liu H. Y., Goncharov A. F., Zhao Z. W., Struzhkin V. V., Mao H. K., Gavriliuk A. G. and Chen X. J., *Phys. Rev. B*, **99** (2019) 024111.
[14] Bera A., Singh A., Muthu D. V. S., Waghmare U. V. and Sood A. K., *J. Phys. Condens. Matter*, **29** (2017) 105403.
[15] Yang L., Dai L., Li H., Hu H., Liu K., Pu C., Hong M. and Liu P., *AIP Adv.*, **9** (2019) 065104.
[16] Rifliková M., Martoňák R. and Tosatti E., *Phys. Rev. B*, **90** (2014) 035108.
[17] Caramazza S., Collina A., Stellino E., Ripanti F., Dore P. and Postorino P., *Eur. Phys. J. B*, **91** (2018) 35.
[18] Congeduti A., Postorino P., Nardone M. and Buontempo U., *Phys. Rev. B*, **65** (2001) 014302.
[19] Roy P., Rouzières M., Qi Z. and Chubar O., *Infrared Phys. Technol.*, **49** (2006) 139.
[20] Voute A., Deutsch M., Kalinko A., Alabarse F., Brubach J. B., Capitani F., Chapuis M., Ta Phuoc V., Sopracase R. and Roy P., *Vib. Spectrosc.*, **86** (2016) 17.
[21] Wieting T. J., Grisel A. and Lévy F., *Phys. B+C*, **99** (1980) 337.
[22] Cappelluti E., Benfatto L., Manzardo M. and Kuzmenko A. B., *Phys. Rev. B*, **86** (2012) 115439.
[23] Fano U., *Phys. Rev.*, **124** (1961) 1866.